Simulating the transition from shallow to deep convection across scales: the role of congestus clouds

Aude Champouillon, Catherine Rio, Fleur Couvreux

Simulating the transition from shallow to deep convection across scales: the role of congestus clouds

Aude Champouillon,[a] Catherine Rio,[a] and Fleur Couvreux[a]

[a] *CNRM, Université de Toulouse, Météo-France, CNRS, Toulouse, France*

Corresponding author: Aude Champouillon, aude.champouillon@polytechnique.org

ABSTRACT: An idealized case of gradual oceanic transition from shallow to deep convection based on Kuang and Bretherton (2006) is simulated at three different horizontal resolutions: one that resolves most of the turbulent eddies, one typical of cloud-resolving models and one typical of general circulation models. The former serves as a reference, and allows the identification of clouds as individual objects, distinguishing shallow cumulus, congestus and cumulonimbus. At coarser resolutions, parameterizations of convection are included and assessed, with a particular focus on congestus clouds and precipitation associated with shallow convective clouds. Congestus clouds are found to contribute the most to turbulent transport during the transition, while occupying a volume comparable to shallow cumulus and cumulonimbus. Kilometer-scale horizontal resolutions prove to be insufficient to resolve congestus, and parameterization schemes of shallow and deep convection are not necessarily appropriate to represent those intermediate clouds. The representation of rainfall in the shallow convection scheme plays a key role in the transition. Sensitivity experiments show that enhanced rainfall inhibits convection in single-column simulations, while it favors resolved convection and spatial heterogeneities in three-dimensional simulations with kilometer-scale resolution. Results highlight the need for an appropriate parameterization of congestus in both kilometer-scale and large-scale models. The case study and the methods presented here are proposed as a useful framework to evaluate models and their parameterizations in a shallow-to-deep convection transition context.

1. Introduction

The representation of the transition from shallow to deep convection remains a challenge for weather forecast and climate models. Indeed, convection is considered sub-grid scale at grid-spacing greater than 50 km and has to be fully parameterized, while it is partially resolved at kilometer-scale resolution (Freitas et al. 2020; Kwon and Hong 2017), and almost entirely resolved only at grid-spacing of the order of 100 m (Jeevanjee 2017; Panosetti et al. 2020). The smallest structures however require a direct numerical simulation (grid-spacing of the order of 1 m or less) to be fully resolved. Since the study of Guichard et al. (2004), that highlighted the difficulties of models with parameterized convection to simulate this transition, several developments have been undertaken to improve this aspect in large-scale models, with a particular focus on the diurnal cycle of precipitation over land. Ways of improving it include a better representation of the shallow convection phase and the impact of cold pools under precipitating systems (Rio et al. 2009), a revisit of the entrainment and detrainment rates formulation (Stirling and Stratton 2012), an adaptation of the CAPE closure for shallow convection to take into account boundary-layer forcing (Bechtold et al. 2014), a unified representation of shallow and deep convection (Park 2014a,b; Park et al. 2019; Suselj et al. 2019, 2022; Smalley et al. 2022; D'Andrea et al. 2014), or the addition of a congestus mode between the shallow and deep ones (Freitas et al. 2021). This has led to some improvement in the representation of the timing of maximum precipitation over land (Couvreux et al. 2015; Tang et al. 2021). Most of those studies, however, have focused more on the delay of precipitation than a better representation of the associated clouds.

The transition is identified to be driven to a large extent by the moistening of the troposphere, whether it is over land (Chaboureau et al. 2004) or over the ocean (Kuang and Bretherton 2006). Waite and Khouider (2010) show that lower-tropospheric moistening could be attributed to the detrainment of water vapor from congestus clouds. Combining observations and large eddy simulations (LES) of the tropical Atlantic, Hohenegger and Stevens (2013) rather state that vertical motion is induced by large-scale disturbances and that the moistening primarily occurs because of moisture convergence. Other studies have emphasized the role of cold pools created by the evaporation of precipitation. Using a LES of a continental case of transition from shallow to deep convection, Khairoutdinov and Randall (2006) highlight that the growth of deep clouds is supported by big thermals generated by precipitation and the associated cold pools. In addition, the spatial

organization of convective clouds has been shown to be strongly influenced by the presence of cold pools (Kurowski et al. 2018). Based on observations and LES of a continental case of convection, Mechem and Giangrande (2018) also aim at identifying what controls the transition from shallow cumulus to congestus. They find good agreement between positive in-cloud buoyancy and high cloud top, and conclude that in-cloud buoyancy could be regarded as a control of the transition.

In this study, rather than analyzing the processes driving the transition, we focus on the role played by the different types of clouds, and more specifically their contribution to vertical turbulent transport.

While shallow cumulus and deep cumulonimbus clouds are known to be the most prominent cloud types in the Tropics, Johnson et al. (1999) emphasize the trimodal distribution of convective clouds during the Coupled Ocean–Atmosphere Response Experiment (COARE) experiment, with congestus clouds representing half of precipitating clouds and contributing one quarter of the total convective rainfall. Also often referred to as towering cumulus, cumulus congestus are precipitating clouds with cloud tops usually reaching up to 6 to 7 km (Kumar et al. 2013).

Traditionally, parameterizations of shallow convection are evaluated with respect to a LES reference (Siebesma et al. 2003; Rio and Hourdin 2008), while deep convection schemes are evaluated against cloud-resolving models, here understood as models with kilometer-scale horizontal resolution (Guichard et al. 2004; Bechtold et al. 2004). As it covers both regimes, explicitly simulating the transition from shallow to deep convection requires a sufficiently fine horizontal resolution to resolve shallow cumulus, and a sufficiently large domain to allow deep convective clouds to develop. Using such a simulation as a reference, it is then appropriate to compare it to (i) simulations with horizontal resolution typical of climate models where convection is fully parameterized, and (ii) kilometer-scale models that resolve the deep convection, typical of regional numerical weather prediction (NWP) models.

Recently, the transition from shallow to deep convection has been studied over land in observational studies based for instance on the GOAmazon field campaign (Zhuang et al. 2017; Tian et al. 2021) or the Holistic Interactions of Shallow Clouds, Aerosols and Land Ecosystems (HI-SCALE) field campaign (Fast et al. 2019). Observational studies over ocean are often related to the study of the Madden-Julian oscillation as in Del Genio et al. (2015); Xu and Rutledge (2016) where large-scale forcing plays an important role. Here, following Kuang and Bretherton (2006), we use

a LES of an idealized case of slow transition over the ocean, mainly forced by the surface. This high resolution simulation allows us to identify different cloud populations and their respective role in the transition. We pay special attention to the congestus, and try to determine implications for the parameterization of this type of clouds. The issue of the representation of the transition in models with parameterized convection is addressed by simulating this case at two other horizontal resolutions, typical of climate models and regional NWP models.

In section 2, we describe the case study, the model and its set-up used for the simulations, as well as the parameterizations involved. In section 3, we present the general results of the main simulations. In section 4, we focus on congestus clouds and their role in the transition. In section 5, we evaluate the representation of the transition in models with parameterized convection. Section 6 is a brief summary of the findings and implications for the further development of parameterizations.

2. Methodology

a. Set-up and model

1) Case study

The simulated case study is inspired by the idealized transition case proposed by Kuang and Bretherton (2006). The initial situation is an oceanic trade cumulus case, derived from observations obtained during the Barbados Oceanography and Meteorology Experiment (BOMEX). We use the initial profiles of potential temperature and water vapor mixing ratio between the surface and 3 km from Siebesma et al. (2003), and we extend them up to 20 km as shown in Fig. 1(a). To force the transition from shallow to deep convection, we use the same procedure as Kuang and Bretherton (2006). We start with the surface heat fluxes described by Siebesma et al. (2003). After 12 hours of simulation, the surface heat fluxes are gradually increased up to 36 hours of simulation, keeping the Bowen ratio constant (Fig. 1(b)). The same large-scale forcing as the one in Siebesma et al. (2003) is applied throughout the simulation.

This set-up allows a slow transition from shallow to deep convection, in order to study a progressive, non-discrete oceanic transition, rather than a rapid continental transition, strongly influenced by the diurnal cycle. We run the simulation during 120 hours. Here, we keep the same wind initial conditions as Siebesma et al. (2003), while Kuang and Bretherton (2006) started with no horizontal wind.

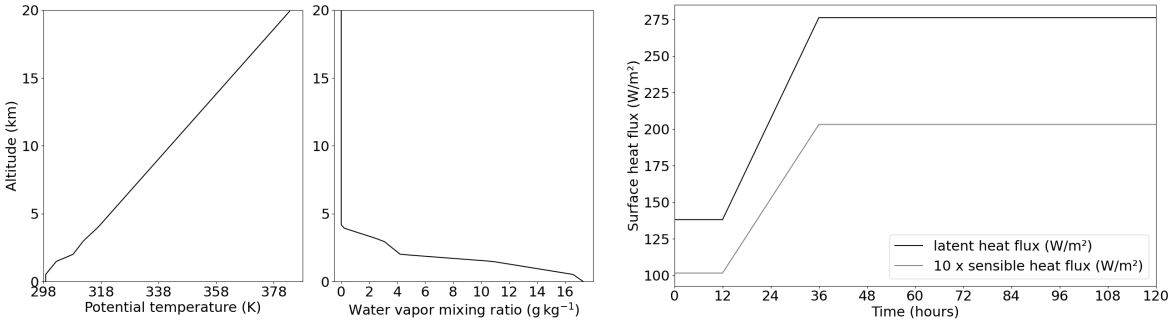

FIG. 1. (a) Vertical profiles of potential temperature and water vapor mixing ratio used as initial conditions. (b) Time-evolution of the prescribed surface sensible and latent heat fluxes

2) MESO-NH

The case study is simulated with the Meso-NH model (Lafore et al. 1998; Lac et al. 2018). Meso-NH is a non-hydrostatic meteorological research model, that can be used for a broad range of configurations. The model uses the anelastic equations of motion with bulk microphysics. Its prognostic variables are the three components of velocity, potential temperature, and six mixing ratios (water vapor r_v, liquid water r_c, rain r_r, ice r_i, snow r_s, graupel r_g). The momentum components are advected with a fourth-order centered scheme, the piece-wise parabolic method scheme is used for the scalar variables and a fourth-order explicit Runge–Kutta method is applied for the temporal discretization.

This model is used to simulate the transition at three different horizontal resolutions, one that resolves most of the eddies, one that resolves deep clouds and one typical of general circulation models where the convective processes are entirely sub-grid. All simulations use the same vertical resolution, a vertical stretched grid of 118 levels with grid-spacing finer than 50 m in the boundary layer and up to 2 km, and coarser higher up (reaching 250 m at the top of the model at 20 km).

We briefly mention here the parameterizations used by all three configurations, and the convective schemes are described further, but more detailed descriptions can also be found in Lac et al. (2018).

The turbulence scheme is based on Redelsperger and Sommeria (1981) and implemented in Meso-NH according to Cuxart et al. (2000). It is based on a prognostic equation for sub-grid kinetic energy. It can be used in its 1D or 3D-form with different mixing lengths.

Microphysical processes are parameterized by a one-moment mixed-phase scheme, denoted as ICE3 (Pinty and Jabouille 1998). It includes five water species: cloud droplets, raindrops, ice crystals, snow or aggregates, and graupel.

No parameterization of radiation is included.

3) The reference simulation

The transition case is first simulated at a horizontal grid-spacing of 100 m within a 50 km x 50 km double periodic domain. Compared to Kuang and Bretherton (2006), the domain is four times larger, in order to allow the deep convection regime to develop freely, but the grid-spacing is twice coarser. At this resolution, we assume that most clouds are explicitly resolved, and hence no parameterization of convection nor sub-grid condensation is introduced. In this LES, we use the 3D-version (horizontal gradients are taken into account) of the turbulence scheme with a length scale proposed by Deardorff (1980) which is a function of the 3D grid size, possibly reduced close to the surface or in stable conditions. To initiate horizontal heterogeneities, a white noise is introduced at the first atmospheric level, with a standard deviation of 0.1 K.

Throughout this study, the LES serves as a reference for comparison with the simulations with parameterized convection.

b. Simulations with parameterized convection

1) Cloud-resolving models

We then run a series of simulations with a 2.5 km horizontal grid-spacing, named CRM for cloud-resolving model. The 250 km x 250 km domain has double periodic boundaries, and the vertical grid is the same as in the LES. A previous version with a 50 km x 50 km domain as the LES led to one single large self-aggregated cloud, not present in the LES. To avoid this phenomenon which was not the focus of the study, the domain has been extended. At 2.5 km grid-spacing, only shallow convection is parameterized while deep convection is still considered resolved. The turbulence scheme is used in its 1D-mode with the Bougeault-Lacarrère (BL89) non-local mixing length, defined by Bougeault and Lacarrere (1989). To initiate horizontal heterogeneities, a white noise is introduced at the first atmospheric level, with a standard deviation of 0.1 K.

The shallow convection scheme, denoted as EDKF, is based on the parameterization of dry updrafts and shallow cumulus described in Pergaud et al. (2009). In this eddy-diffusivity / mass-flux (EDMF) parameterization, one resulting updraft, described by the mass flux, represents the collective effect of several plumes. The cloud ensemble is considered in steady state and the vertical evolution of the mass flux is defined by entrainment and detrainment. This allows one to determine the evolution of updraft conservative variables such as liquid potential temperature θ_l and total water mixing ratio r_t during ascent. The vertical evolution of the updraft vertical velocity is also computed considering buoyancy as a source term, and entrainment and pressure as a sink. The scheme starts at the surface, where the mass flux is determined from the buoyancy flux and the BL89 upward mixing length. The updraft fraction (a_u) is diagnosed at each level following the independent computation of the updraft mass flux M_u and the updraft vertical velocity w_u, using $a_u = \frac{M_u}{\rho w_u}$. It is used to determine the associated cloud fraction $CF = 2.5a_u$. The updraft liquid mixing ratio r_{cu} is calculated from the conserved variables, and used to determine the grid cell liquid mixing ratio $r_c = r_{cu}CF$. Hence, if the mass flux were zero in a grid cell, then that grid cell would be cloud-free. Note that this refers only to the liquid mixing ratio and the associated cloud originating from the shallow convection scheme. Both the turbulence and the microphysics schemes can also contribute to the total cloud.

Meso-NH includes an artificial vertical limitation of EDKF: when the diagnosed cloud exceeds 4 km in depth, the mass flux is multiplied by a coefficient such that it linearly decreases between 3 km and 4 km of depth, and reaches zero above. As it is, EDKF is hence not designed to represent clouds deeper than 4 km, which will have to be either resolved in CRM mode or parameterized by a deep convection scheme in the single-column simulations described in the next paragraph.

2) Single-column simulations

Finally, a series of single-column (1D) simulations is run with the same vertical grid, which is rather unusually fine for a GCM set-up. An additional single-column simulation was run with 87 vertical levels, but shows little sensitivity to vertical resolution (not shown).

In this 1D configuration, both shallow and deep convection are parameterized, using the same turbulence scheme and the same shallow convection scheme as in the CRM simulations. The deep convection scheme, denoted as KAFR, is based on Bechtold et al. (2001). The scheme is based on

the decomposition of a grid cell into an updraft, a downdraft and the environment. The updraft and the downdraft are described by the associated mass fluxes whose evolution relies on entrainment and detrainment. An updraft is generated from a parcel rising from the surface if:

- At the lifting condensation level, the virtual potential temperature of the rising air parcel is greater than the virtual potential temperature of the environment plus a threshold dependent on the vertical velocity and the grid size.
- The resulting cloud is deeper than 3 km.

If one of those two conditions is not fulfilled, the same procedure is repeated with the air parcel above, and so on. The intensity of convection is controlled by a closure based on CAPE. It makes use of the assumption that all CAPE in a grid cell is consumed within a given adjustment period of 1 hour in the simulations presented here.

Table 1 summarizes the three levels of resolution and the corresponding parameterizations. Note that KAFR depends explicitly on the grid-spacing through the trigger function and the relaxation time used in the CAPE closure, while EDKF does not incorporate any grid-size dependence.

3) Sensitivity tests

For both the CRM and the 1D set-ups, we perform two different simulations, to account for different parameterization options. A reference simulation, called *ref*, is used as the default configuration, and a simulation called *new microphysics* includes an additional feature in the shallow clouds parameterization. In this option, the cloud-to-rain autoconversion threshold is applied to the updraft liquid mixing ratio (r_{c_u}) instead of the grid cell liquid mixing ratio (r_c). Similarly, the evaporation rate is determined from the rain mixing ratio in the precipitating fraction instead of the grid cell rain mixing ratio.

In 1D, we perform another series of sensitivity tests, to assess whether allowing the shallow convection scheme to represent deeper clouds, or adjusting the parameterization of precipitation associated with shallow convection, improves the representation of the transition to deep convection. In *1D lim 6km*, we start from *1D ref* and change the upper limit of the EDKF scheme to allow it to represent deeper clouds. In *1D rain sensitivity*, we start from *1D new microphysics* and adjust the cloud-to-rain autoconversion threshold to slightly reduce the ability of shallow clouds to produce precipitation.

Name	Hor. grid-spacing	Domain size	Turbulence	Shallow conv.	Deep conv.	Microphysics
LES	100 m	50 km × 50 km	DEAR 3D	resolved	resolved	ICE3
CRM	2.5 km	250 km × 250 km	BL89	EDKF	resolved	ICE3
1D	50 km	50 km × 50 km	BL89	EDKF	KAFR	ICE3

TABLE 1. Summary of the 3 types of simulation and their characteristics and parameterizations

Name	Details	Applied in
ref	configuration of reference	1D and CRM
new microphysics	change in parameterization of cumulus microphysics (cloud and precipitation fractions taken into account for precipitation and evaporation diagnosis)	1D and CRM
lim 6km	EDKF limitation set to 6 km instead of 4 km	1D
rain sensitivity	change of the cloud-to-rain autoconversion threshold	1D
no EDKF	EDKF deactivated	1D and CRM

TABLE 2. Summary of all simulations with parameterized convection

Entrainment is known to play a key role in cloud deepening and is usually different in shallow and deep convection schemes, entrainment being stronger for shallow convection. Additional sensitivity tests have been carried out to document the impact of the mixing formulations on the transition, modifying the intensity of the entrainment rate separately in EDKF and KAFR. Those experiments show little impact of these modifications on the representation of the transition in 1D (not shown), but other mixing formulations might behave differently.

Finally, in both CRM and 1D modes, we run a simulation without any shallow convection scheme, allowing only the turbulence scheme to represent boundary-layer mixing (*no EDKF* simulations), to evaluate the added value of the EDMF shallow convection scheme.

The names and descriptions of the simulations run in the CRM and 1D configurations are summarized in table 2.

3. Simulating the transition from shallow to deep convection across scales

a. Transition in LES

This section focuses on the representation of the transition in the LES simulation. Figure 2 gives an overview of the time evolution of the potential temperature and water vapor mixing ratio tendencies as well as the precipitating and non-precipitating hydrometeors.

To analyze the transition more precisely, we identify four phases. Between 6 and 12 hours, named the *shallow convection regime* period (S), the cloud layer shows limited vertical growth. The potential temperature tendency is slightly positive (close to $0.05\,\mathrm{K\,h^{-1}}$) except at cloud top where the updraft's overshoot produces a slightly negative tendency (close to $-0.2\,\mathrm{K\,h^{-1}}$). The vapor mixing ratio tendency is also very weak, positive in the cloud layer and negative below (about $0.07\,\mathrm{g\,kg^{-1}\,h^{-1}}$ in absolute value). Between 12 and 60 hours, named the *first transition phase* (T1), we observe a direct response to the increasing surface fluxes, namely a progressive elevation of the top of the cloud layer, and strong negative potential temperature tendency and positive vapor tendency in the upper part of the cloud layer. Between 60 hours and 90 hours, referred as the *second transition phase* (T2), the growth of the cloud layer slows down, the moistening and cooling of the top of the cloud layer decrease, but precipitation intensifies. Then, from 90 hours to the end of the simulation (120 hours), named the *deep convection regime* period (D), the tendencies and the cloud top show an intermittent evolution, with some abrupt and strong variations. Cloud tops reach 12 km during this phase similarly to Kuang and Bretherton (2006). Precipitation first appears around 25 hours, in the middle of the first transition phase. It only reaches the surface around 50-60 hours, roughly at the beginning of the second transition phase. Precipitation becomes intermittently more intense from 90 hours, with peaks reaching 4 to 5 mm $\mathrm{day^{-1}}$ consistently with Kuang and Bretherton (2006). The 0°C isotherm (Figs. 2(c) and 2(d)) indicates approximately above which altitude the water components can freeze. Clouds contain ice crystals only from the end of the second transition phase.

Figure 3 gives an overview of the spatial organization of the clouds. At 8 hours (shallow convection regime), clouds are shallow and homogeneously distributed on the horizontal. At 35 hours (first transition phase), clouds become deeper, but the spatial distribution remains relatively unorganized. At 74 hours (second transition phase), clouds are deeper and start organizing in clusters. At 105 hours (deep convection regime), large clear sky areas have been created while one cluster of deep clouds dominates the population. To get a better three-dimensional view of the simulated clouds and illustrate their vertical development throughout the transition, virtual images of the scenes are produced, using the tool *htrdr-atmosphere*, a Monte-Carlo radiative transfer simulator (Fig. 3, lower row).

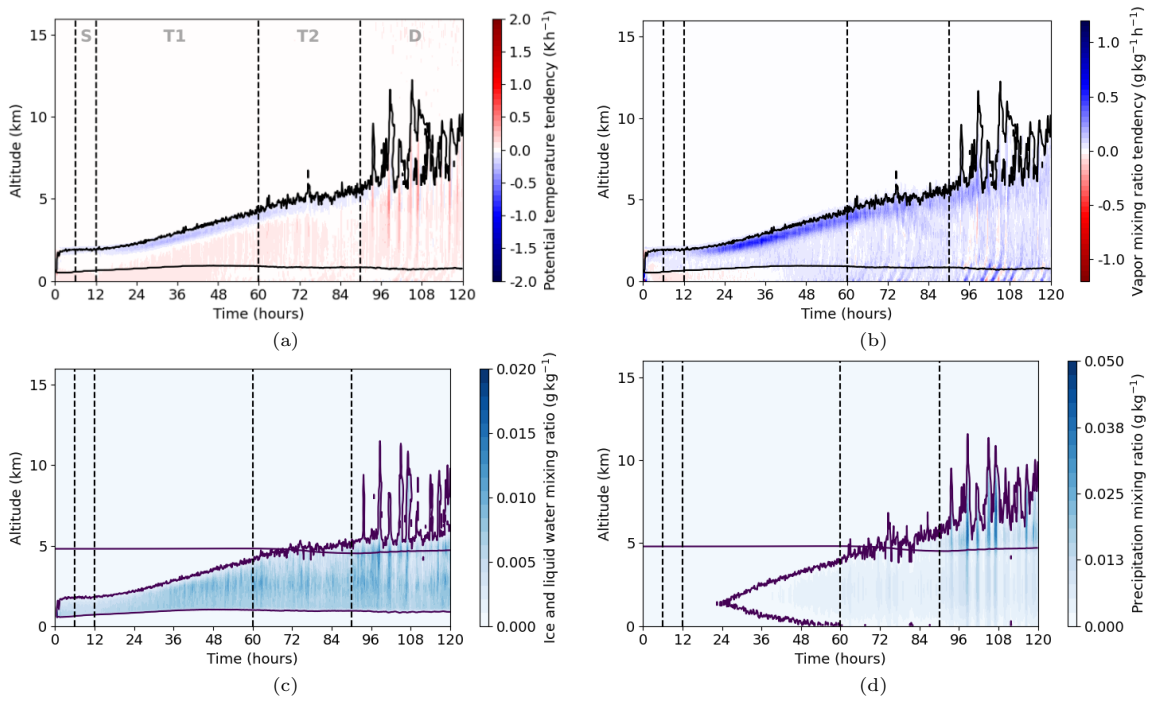

FIG. 2. Time evolution of the mean vertical profiles of the LES. The vertical dashed lines delimit the different phases. (a) Filled contour: potential temperature tendency. Line contour: level of zero cloud fraction. (b) Filled contour: vapor mixing ratio tendency. Line contour: level of zero cloud fraction. (c) Filled contour: liquid and ice water mixing ratio. Line contour: 10^{-6} kg kg^{-1} level. Horizontal line: altitude of the 0°C isotherm. (d) Filled contour: rain, snow and graupel mixing ratio. Line contour: 10^{-6} kg kg^{-1} level. Horizontal line: altitude of the 0°C isotherm.

b. Transition in simulations with parameterized convection

Figure 4 provides a first insight of how the transition is represented in 1D and CRM modes. Up to 82 hours, *1D ref* and *CRM ref* have similar mean profiles, consistent with the fact that shallow convective processes are represented by the same scheme. They reproduce the tendencies and the development of the cloud layer simulated in the LES quite well, except for tendencies that are too strong at the top of the cloud layer. In 1D, larger differences from the LES emerge at 91 hours, when the cloud layer reaches the 4 km depth limitation of EDKF, and microphysical processes cause strong tendencies. By examining tendencies budget terms, we identify the start of the deep convection scheme to occur around 109 hours, 19 hours later than the beginning of the deep convection regime in the LES. In the CRM, at 82 hours, a deep convection regime abruptly

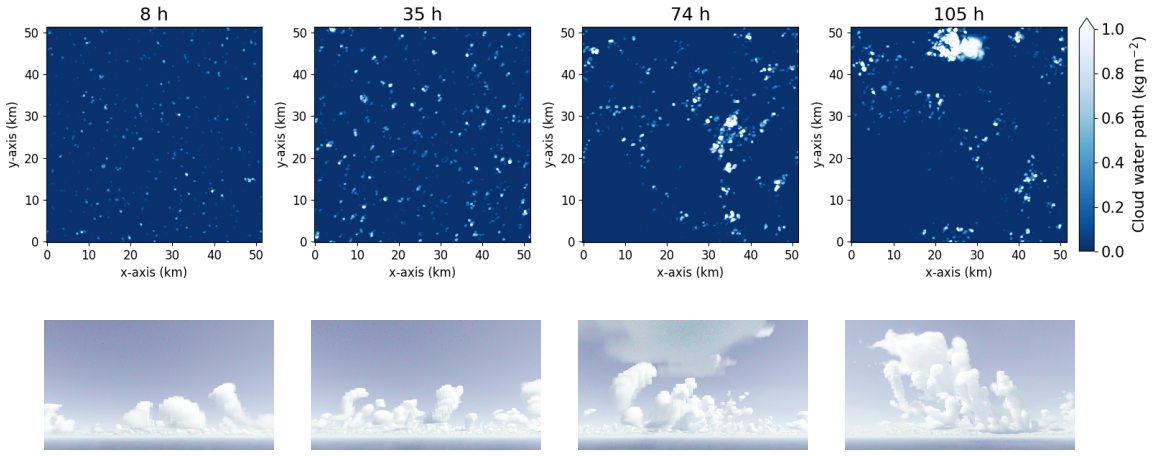

FIG. 3. Upper row: Cloud (liquid + ice) water path at 4 different times. White color indicates values of 1 kg m^{-2} or more. Lower row: Virtual image of the scene at 8 hours, 35 hours, 74 hours, 105 hours. The images were rendered by *htrdr-atmosphere* (Villefranque et al. 2019). Position of the camera relative to its target in km in the (x,y,z)-reference system: (0,-16,-5.5). Vertical field of view: 45°. The highest clouds have their top up to 2,100 m at 8 hours, 2,900 m at 35 hours, 5,000 m at 74 hours and 11,000 m at 105 hours.

activates with a cloud layer developing up to 16 km. Simultaneously, intense precipitation forms, reaching the surface instantaneously and leading to evaporation-driven tendencies in the sub-cloud layer. Precipitation reaches a total of 6.5 mm, against 2.5 mm in the LES. In 1D, precipitation forms from 92 hours and reaches 0.6 mm at the end of the simulation. Both in the CRM and in 1D, precipitation occurs too late compared to the LES.

Effects of the modified microphysics in both *1D new microphysics* and *CRM new microphysics* are shown in Fig. 5. Rainfall is expected to be favored when applying the autoconversion threshold on in-cloud water instead of mean water over the grid cell. In 1D, precipitation now forms from the beginning of the simulation, hence too early (Fig. 5(b)), although the accumulated precipitation at the end of the simulation is of the right order of magnitude: 2.25 mm against 2.5 mm in the LES. Compared to *CRM ref*, in *CRM new microphysics*, precipitation starts earlier, around 30 hours (Fig. 5(d)), and its intensity is reduced before the deep convection regime period, but it still reaches 6 mm at the end of the simulation.

It appears that the effects of the same modification in the microphysics scheme are very different in 1D and in CRM mode. In 1D, the increase in precipitation seems to inhibit the convection and

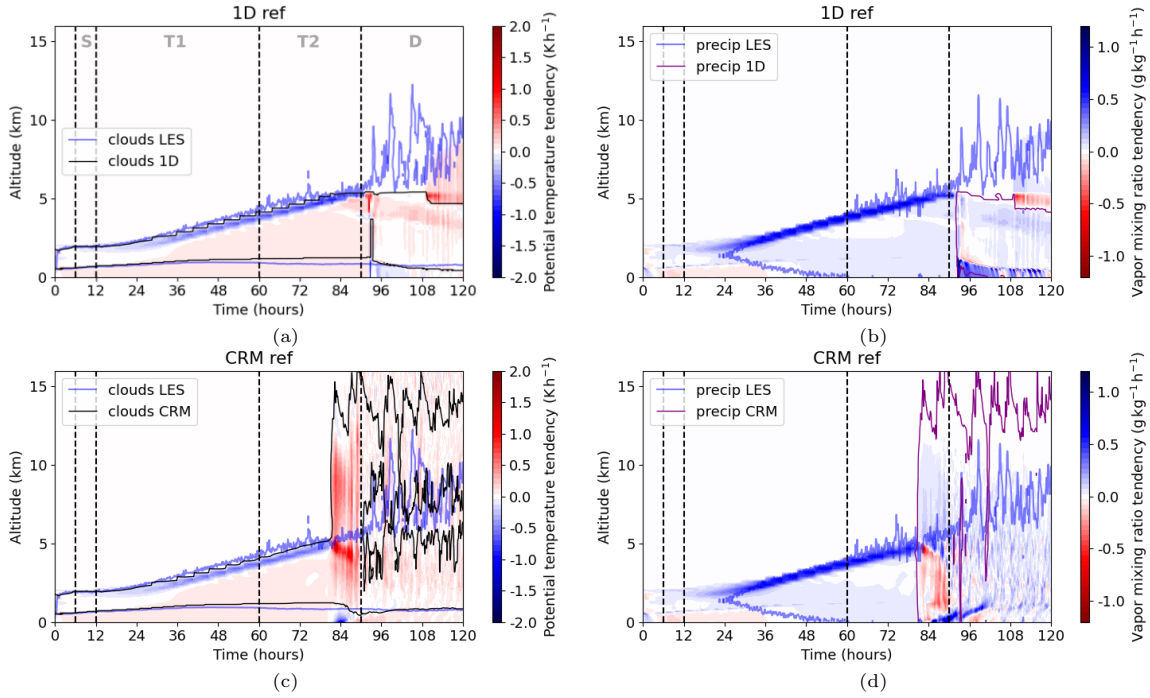

FIG. 4. Time evolution of the mean vertical profiles of (a) and (c) potential temperature tendency with the level of zero cloud fraction and (b) and (d) water vapor mixing ratio tendency with the level of 10^{-6} kg kg^{-1} precipitation mixing ratio for (a) and (b) *1D ref* and (c) and (d) *CRM ref*. In (a) and (c) the blue contour is the level of zero cloud fraction in the LES and in (b) and (d) the blue contour is the level of 10^{-6} kg kg^{-1} precipitation mixing ratio in the LES. The vertical dashed lines delimit the different phases identified in the LES

the vertical growth of the cloud layer, preventing the activation of the deep convection scheme (Fig. 5(a)). On the contrary, the CRM is barely affected until 52 hours when deep convection starts being resolved. The cloud layer experiences from this point stronger positive potential temperature tendency and extends up to the highest levels (Fig. 5(c)). This difference in response will be further addressed in section 5.

Comparing the *ref*-simulations to the *new microphysics*-simulations suggests that precipitation associated with shallow convection might be of great importance in the triggering of a deep convection regime, whether it is parameterized or resolved.

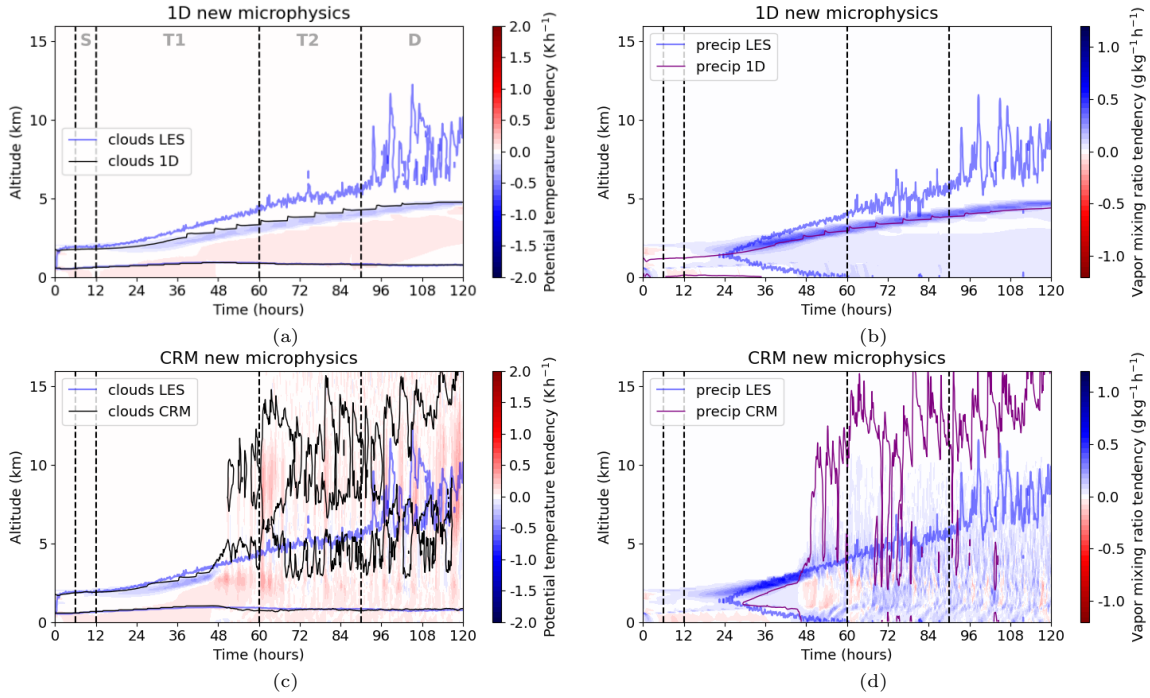

FIG. 5. Time evolution of the mean vertical profiles of (a) and (c) potential temperature tendency with the level of zero cloud fraction and (b) and (d) water vapor mixing ratio tendency with the level of 10^{-6} kg kg^{-1} precipitation mixing ratio for (a) and (b) *1D new microphysics* and (c) and (d) *CRM new microphysics*. In (a) and (c) the blue contour is the level of zero cloud fraction in the LES and in (b) and (d) the blue contour is the level of 10^{-6} kg kg^{-1} precipitation mixing ratio in the LES. The vertical dashed lines delimit the different phases identified in the LES

4. The central role of congestus in the transition

a. Cloud populations simulated by LES

In this part, clouds are identified as individual objects using an object identification and characterization algorithm. This algorithm applies a binary mask on the three-dimensional grid, defined by: "a cell is cloudy if $r_c + r_i > 10^{-6}$ kg kg^{-1} and $w > 0$" where w is the vertical velocity. A cloud is then defined as a set of contiguous cloudy cells. Only objects bigger than 9 cells are kept and for objects that would be at the border of the domain, we make use of the double-periodicity.

Using this algorithm, we identify clouds as isolated objects every hour of the simulation and diagnose for each identified cloud a top (defined as the altitude of the highest grid cell within the object) and a depth (defined as the difference in altitude between the highest and lowest grid cells).

Cloud types	Top	Depth
Cumulus	≤ 3 km	no condition
Congestus	≥ 3 km and ≤ 6 km	≥ 500 m
Cumulonimbus	≥ 6 km	≥ 500 m
Others	≥ 3 km	≤ 500 m

TABLE 3. Classification criteria of clouds identified in the LES

Following the criteria described in table 3, we distinguish four types of clouds: shallow cumulus, congestus, cumulonimbus, and a last type, denoted as *others*.

Although this classification is rather arbitrary, it provides a handy partition of the cloud population. Moreover, each class exhibits rather constant thermodynamic and geometric properties throughout the simulation. 30% of cumulus clouds produce precipitation at the beginning of the simulation and this proportion increases and stabilizes at 50% around 37 hours. 100% of congestus and cumulonimbus are precipitating clouds. From the covered area A of a cloud, an equivalent radius R is defined by $R = \sqrt{\frac{A}{\pi}}$. An aspect ratio r is then defined by $r = \frac{d}{R}$ where d is the depth of the cloud. Within the cumulus and the congestus classes, the mean r remains roughly constant over time. It is about 2 for cumulus and 4 for congestus, showing that that these two types of clouds have quite different shapes. For cumulonimbus, the mean aspect ratio varies greatly around an average of 4, but this is also linked to the fact that there are only a few clouds in this class.

Figure 6(a) shows the number of clouds identified at each hour and for each type. In Fig. 6(b), the volumetric fraction, defined as the ratio of the volume occupied by clouds over the total volume of the domain, is given as a function of time for each cloud type. Shallow cumulus dominate throughout the simulation in terms of population size, and their volumetric fraction is roughly 0.07%. Congestus start to form around 36 hours and their volumetric fraction reaches the one of cumulus at about 60 hours, which coincides with the beginning of the second transition phase. Cumulonimbus appear around 90 hours, at the beginning of the deep convection regime period. They are very sparsely populated but their volumetric fraction is similar to the one of congestus and shallow cumulus during the deep convection regime period. Earlier occurrences of clouds labelled as cumulonimbus may rather be congestus having higher tops than the classification threshold, than evidence of deep convection. The last type of clouds, too high to be considered as shallow

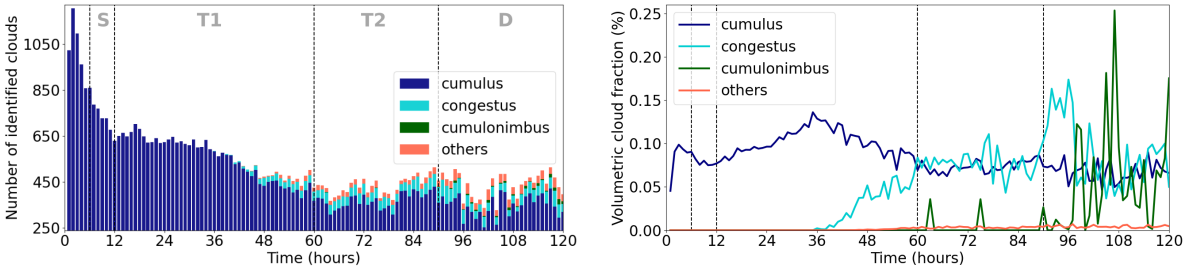

FIG. 6. Time evolution of (a) number of clouds and (b) volumetric cloud fraction of each type of clouds.

cumulus but too thin to be part of the congestus and cumulonimbus types, is present from 48 hours onward but its volumetric fraction remains negligible.

b. Spatial organization

Figure 7 shows the spatial organization of the different cloud types and the temperature anomaly at the first model level at four different times. At 8 hours (shallow convection regime), cumulus clouds are spread quite homogeneously in space, they remain small, and the temperature is almost uniform. At 35 hours (first transition phase), cumulus become slightly bigger and slowly start organizing in clusters. Temperature anomalies are barely noticeable. At 74 hours (second transition phase), large circular areas of clear sky can be seen, mostly corresponding to areas of weak negative temperature anomalies. Congestus clouds are clearly gathered in clusters, mostly located at the edges of cold pools. At 105 hours (deep convection regime), this type of organization remains. There is also a single cumulonimbus co-located with a large and strong cold temperature anomaly.

c. Contribution of each cloud type to turbulent fluxes

For each cloud type, and for the remaining environment defined as cloud-free grid cells, a contribution to turbulent vertical fluxes is calculated. Given a cloud type c defined by an ensemble $C(z)$ of grid cells, its contribution to the turbulent vertical flux of a variable ϕ at altitude z is given by :

$$\overline{w'\phi'}_c(z) = \frac{1}{N} \sum_{(x,y)\in C(z)} (w'\phi')(x,y,z)$$

where N is the number of cells in the horizontal grid, and the prime denotes the anomaly with respect to the domain horizontal mean.

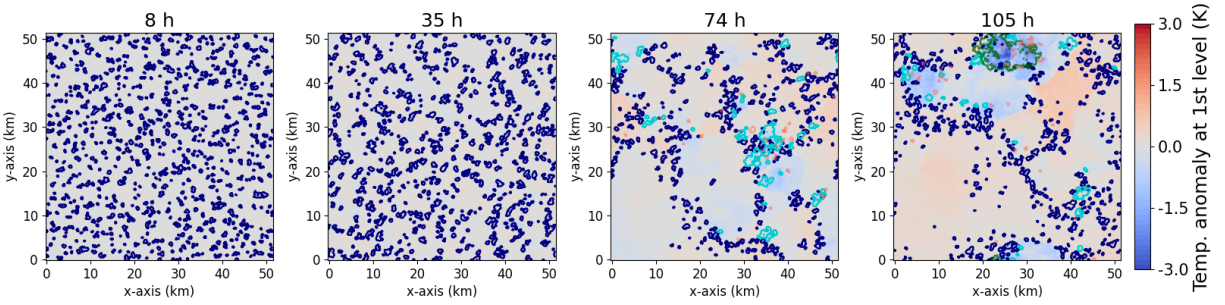

364 FIG. 7. Temperature anomaly at the first model level (filled contour) and identified clouds contours (dark blue:
365 cumulus, light blue: congestus, green: cumulonimbus, orange: others). Three-dimensional masks of each cloud
366 type resulting from the object identification are projected onto two-dimensional masks, and hence visualized as
367 from the top of the atmosphere.

Here we consider the resolved vertical turbulent fluxes of r_t the total water mixing ratio and θ_l the liquid potential temperature since these quantities are the conservative variables in EDKF. These two variables are defined as follows:

$$r_t = r_v + r_c + r_i$$

$$\theta_l = \theta - r_c \frac{L_v}{c_{p,d}} \frac{\theta}{T}$$

371 with θ the potential temperature, T the temperature, L_v the latent heat of vaporization and $c_{p,d}$ the
372 specific heat of dry air. We assume the resolved fluxes of the LES to be close to the total fluxes,
373 except near the surface where the resolved fluxes approach zero.

376 Figure 8 shows the vertical profiles of these contributions time-averaged over the four identified
377 phases. Note that the dry updrafts are included in the environment in this analysis. During the
378 shallow convection regime period, only cumulus are present. During the first transition phase,
379 cumulus still dominate the total turbulent vertical fluxes of both total water mixing ratio and
380 liquid potential temperature, except at altitudes corresponding to the top of cumulus and above.
381 During the second transition phase, the contribution of congestus dominates from about 2.5 km
382 and above, while the contribution of cumulus remains larger at lower altitudes. From Fig. 6(b), we
383 know that during this phase, the volume occupied by these two populations is approximately the
384 same, which legitimizes the comparison of their contributions here. During the deep convection

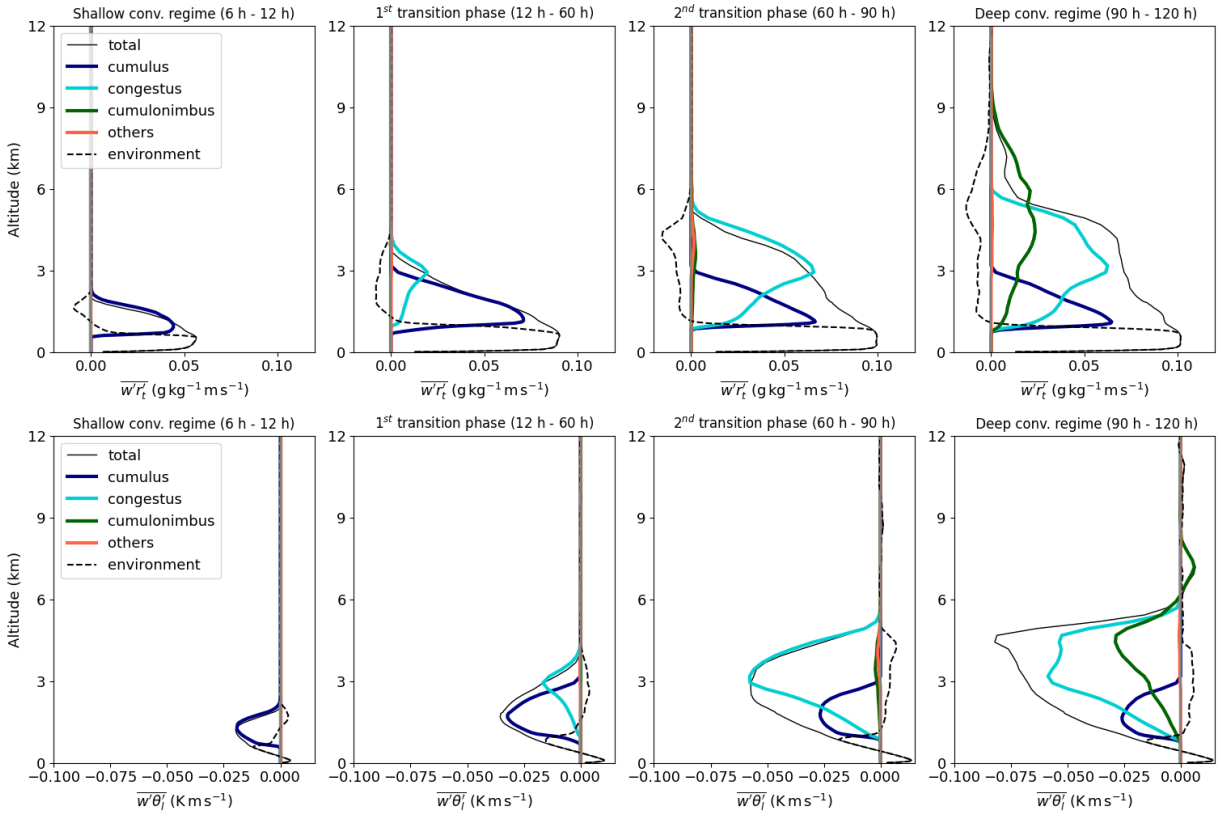

374 FIG. 8. Contribution of each cloud type to resolved vertical turbulent fluxes averaged over the different
375 identified phases of total water mixing ratio (upper row) and liquid potential temperature (lower row).

385 regime period, the contribution of congestus is larger than that of cumulonimbus, although they
386 occupy on average approximately the same volume. At lower altitudes, cumulus continue to have
387 a significant contribution. Finally, as expected, the last category of identified clouds (*others*), does
388 not contribute significantly.

389 This analysis highlights that during the transition from shallow to deep convection, congestus
390 are the main contributors to vertical turbulent fluxes of θ_l and r_t, while occupying a volume as
391 big as cumulus and cumulonimbus. This suggests that representing congestus in simulations with
392 parameterized convection is key to properly simulate the transition. Additionally, cumulus while
393 being shallow clouds still contribute to a significant part of both the fluxes and the cloud fraction
394 during the transition, as well as during the onset of deep convection, and they must therefore also
395 be represented simultaneously to deeper clouds.

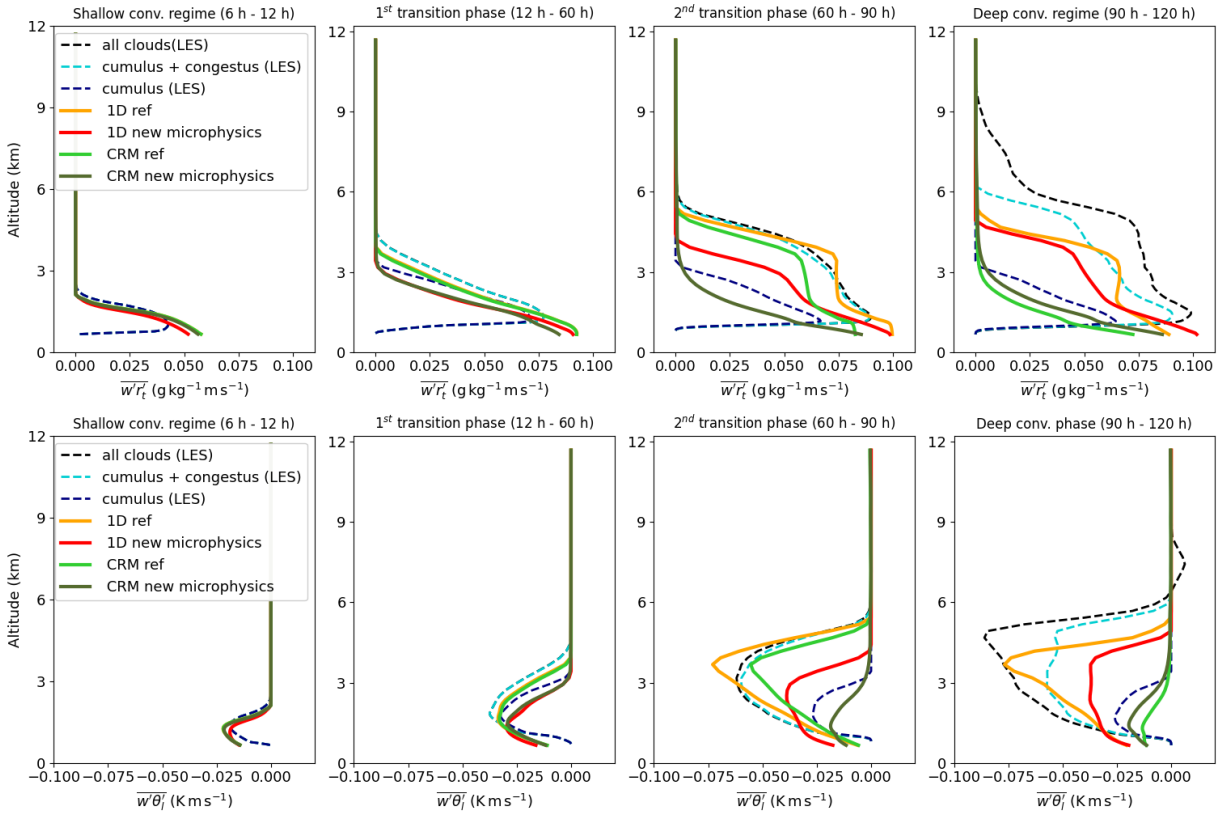

FIG. 9. Contribution to vertical turbulent fluxes of clouds of the LES (resolved) and parameterizations in various 1D and CRM simulations (parameterized) averaged over the different identified phases of total water mixing ratio (upper row) and liquid potential temperature (lower row).

5. Parameterized versus resolved convection across scales

a. Evaluation of parameterized turbulent fluxes against LES

For the CRM and the 1D simulations, we assess the performance of EDKF to represent the shallow regime and the transition to the deep regime, by considering the associated vertical turbulent fluxes. Figure 9 shows the time-averaged fluxes computed by the shallow convection and turbulence schemes (EDMF concept) in the four simulations mentioned previously, compared to the resolved fluxes diagnosed in the LES of cumulus only, both cumulus and congestus, and all clouds. Note that the comparison is not valid either in the dry part of the updrafts or in the lower part of the cloud layer, since the shallow convection scheme considers dry updrafts and clouds without discontinuity, whereas only clouds were identified in the LES.

All simulations capture turbulent fluxes comparable to the LES in the shallow convection regime period and in the first transition phase. In the second transition phase, *1D ref* best represents the vertical turbulent fluxes associated with both cumulus and congestus, although it overestimates θ_l fluxes around 4 km. Fluxes in *1D new microphysics* and *CRM ref* are larger than those of cumulus, but smaller than those of cumulus and congestus together. In this phase, *CRM new microphysics* does not even represent the contribution of cumulus. In the deep convection regime period, fluxes in *1D ref* and *1D new microphysics* are close to those of cumulus and congestus, but still lower, except around 4 km, where *1D ref* overestimates θ_l fluxes. The deep convection scheme activates only at the end of this phase in *1D ref* and does not activate at all in *1D new microphysics*. Therefore, the underestimation of the turbulent transport is not compensated for. In CRM simulations, the shallow convection parameterization contribution is inhibited, underestimating even fluxes of cumulus. However, in this phase, as will be shown later, the resolved fluxes are quite large in the cloud layer.

To summarize, EDKF in *1D ref* performs relatively well in terms of turbulent transport, although not fully reaching the magnitude and the height extent of the contribution of congestus simulated in the LES. Fluxes in *CRM ref* are also in good agreement with the fluxes of the clouds of the LES, except during the last phase. The inhibiting effect on the mass flux scheme of favored precipitation in *new microphysics* is also visible, as both in 1D and in the CRM, the magnitudes of the parameterized fluxes are reduced compared to *ref*.

b. What part of transition is resolved at 2.5 km grid-spacing?

1) Expected resolved fluxes at various scales

While it is known that turbulence and shallow convection must be parameterized for kilometer-scale resolutions, less attention has been paid to the transition from shallow to deep convection and in particular to the congestus phase. In this section, we try to determine at which horizontal scale the convection is well-resolved throughout the transition. For this purpose, we follow a coarse-graining procedure as introduced by Honnert et al. (2011) and also applied by Strauss et al. (2019) and others. Given a grid-spacing Δx, the domain of the LES is divided into square subdomains with a Δx length. The expected resolved vertical turbulent fluxes of a quantity ϕ at a grid-spacing

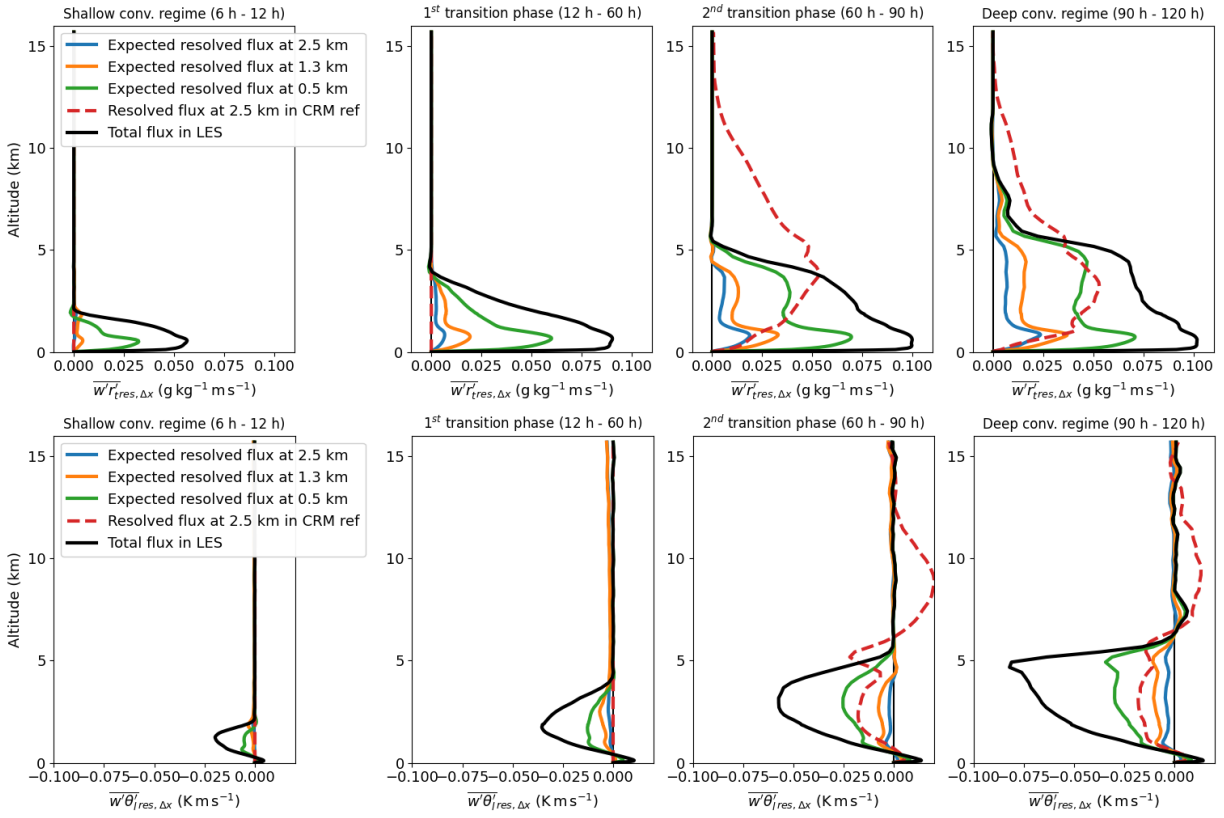

FIG. 10. Expected resolved vertical turbulent fluxes at different resolutions computed from LES, resolved fluxes in *CRM ref* and total fluxes in LES, averaged over the different identified phases of total water mixing ratio (upper row) and liquid potential temperature (lower row).

Δx is assumed to be given by:

$$\overline{w'\phi'}_{res,\Delta x} = \overline{(\overline{w}^{\Delta x} - \overline{w})(\overline{\phi}^{\Delta x} - \overline{\phi})}$$

where the simple overline indicates a horizontal average over the entire domain, and the overline with Δx-subscript indicates a horizontal average over a subdomain of length Δx. The result is a vertical profile for each time step that can be averaged over the four different phases.

Using the LES, this computation is done for Δx = 2.5 km, 1.3 km and 500 m, and the results are shown in Fig. 10 for r_t and θ_l. In the same figure, the total vertical turbulent fluxes resolved in the LES and the vertical turbulent fluxes resolved in *CRM ref* are shown as well, for comparison.

This analysis shows that at a grid-spacing of 2.5 km, the vertical turbulent transport is poorly resolved, even in the deep convection regime period. It questions the assumption that simulations in CRMs should allow the deep convection phase to be resolved. It also shows that in *CRM ref*, the resolved part is null during the first half of the simulation and overestimated at high altitudes during the second half.

2) Resolved versus parameterized clouds in CRM

In this part, we investigate the spatial organization of resolved and parameterized clouds in relation to near-surface heterogeneities in the CRM simulations. Figure 11 allows one to visualize the position of resolved clouds with the temperature anomalies at the first model level at four different times.

The most striking difference between *CRM ref* and *CRM new microphysics* is the delay in meso-scale organization simulated in the former compared to the latter. They both exhibit almost uniform temperature at the first model level and a cloud layer without significant water content at the beginning of the simulation. In *CRM ref*, the first resolved clouds appear shortly before 80 hours, just before the beginning of precipitation (81 hours). At 105 hours (Fig. 11), temperature anomalies are clearly established in *CRM ref*, together with large resolved clouds, although their water content remains mostly low. In *CRM new microphysics*, the first resolved clouds appear at 48 hours, about 20 hours after the onset of precipitation, and approximately when it reaches the surface. This could indicate that the early occurrence of rainfall enhances horizontal heterogeneities of temperature, facilitating resolved circulation, which in turn increases horizontal heterogeneities in cloud development. At 48 hours (Fig. 11), resolved clouds are located above cold temperature anomalies of about 1 K, and are circled by parameterized clouds (visible in water content). This could suggest that the meso-scale organization of parameterized clouds drive the spatial organization of resolved clouds.

Keeping in mind that the domain in these simulations is 25 times larger than in the LES, Fig. 11 can be compared to Fig. 3 and Fig. 7. Patterns of temperature anomaly are significantly larger in the CRM simulations than in the LES, but they do have a similar organization relative to the clouds, since all resolved clouds are spatially and temporally associated with strong negative temperature anomalies, similarly to congestus and cumulonimbus in the LES.

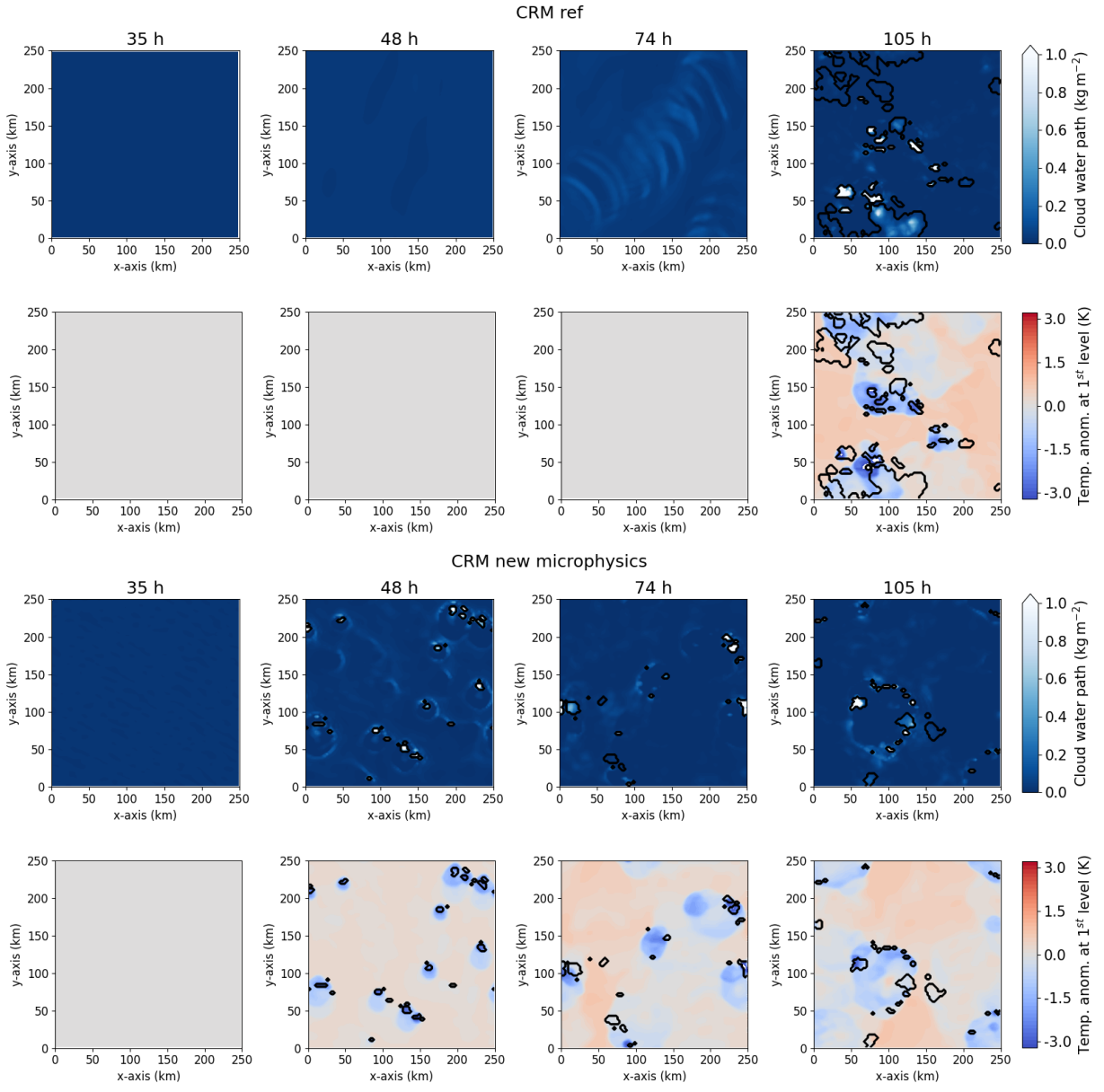

FIG. 11. Cloud (liquid + ice) water path (filled contour, white color indicating values of 1 kg m^{-2} or more) and resolved cloud edges (black line contour), and temperature anomaly at the first model level (filled contour) and resolved cloud edges (black line contour) in *CRM ref* (two upper rows) and *CRM new microphysics* (two lower rows).

Columns of resolved clouds are defined as columns where at least one level has a cloud fraction of 1 and verifies $r_c + r_i > 10^{-6}$ kg kg^{-1}.

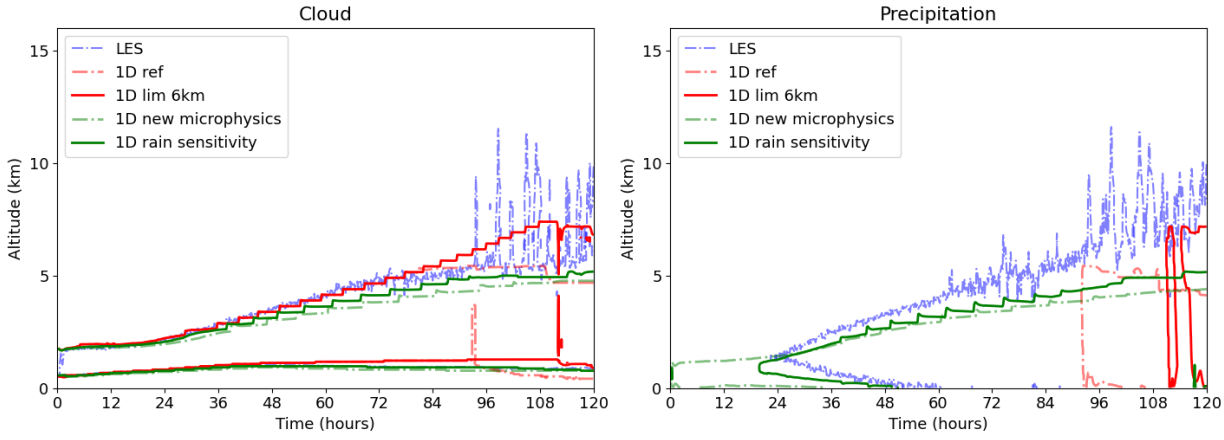

FIG. 12. Time evolution of the mean vertical profile of (a) cloud contour and (b) precipitation contour, in the LES (blue) and the different 1D sensitivity tests. Cloud and precipitation contours correspond to the 10^{-6} kg kg^{-1} level of respectively liquid plus ice mixing ratio and rain plus snow plus graupel mixing ratio.

c. How to parameterize congestus clouds?

1) LET SHALLOW CONVECTION GROW DEEPER

To investigate whether a shallow convection scheme could represent congestus clouds, EDKF is modified in order to let clouds grow deeper than 4 km, namely up to 6 km. The corresponding 1D simulation is called *1D lim 6km*. As shown in Fig. 12, increasing the limitation of EDKF allows deeper clouds to develop and consequently transport heat and moisture higher up (not shown), in better agreement with the LES than *1D ref*. However, precipitation in this simulation appears only at 112 hours, against 93 hours for *1D ref* and 22 hours for the LES. This shows that the shallow convection scheme can grow clouds as deep as the congestus, but has difficulties representing correctly the associated precipitation.

2) THE INFLUENCE OF SHALLOW CLOUDS PRECIPITATION

The simulation *1D new microphysics* has revealed the major role of precipitation under shallow clouds. In *1D rain sensitivity*, we modify the cloud-to-rain autoconversion threshold so that precipitation appears at the same time as in the LES, namely 22 hours. Precipitation in *1D rain sensitivity* appears at 20 hours, and reaches the surface at 50 hours (Fig. 12(b)), which is about the same time as in the LES. The accumulated precipitation at the surface reaches a bit less than 2 mm (against 2.5 mm in the LES). However, even if the vertical development is slightly less inhibited

than in *1D new microphysics* (Fig. 12(a)), it remains too shallow and the deep convection scheme still does not activate. This confirms that the additional rainfall during the first transition phase inhibits the mass-flux scheme, and without resolved circulation as in the CRM, in 1D simulations, it limits the development of deeper clouds such as congestus.

3) Can turbulence do everything?

To illustrate further the role of the shallow convection scheme and similarly to Barber et al. (2022), simulations are run without any shallow convection scheme both in 1D and CRM configurations (*1D no EDKF* and *CRM no EDKF*). The effect of removing the shallow convection scheme differs greatly between these two configurations.

In *1D no EKDF*, as shown in Fig. 13(a), the vertical development of clouds is not sufficient. Moreover, values of cloud fraction are close to 1 within the whole cloud layer and the liquid water mixing ratio is about 10 times too large compared to the horizontal mean in the LES. Precipitation is also not well represented in this simulation, as shown in Fig. 13(b), as it appears too late. The precipitation rate is also too high, with values fluctuating around 0.5 mm h^{-1} and up to 1.5 mm h^{-1}, while in the LES it never exceeds 0.2 mm h^{-1}.

In *CRM no EDKF* (Figs. 13(a) and (b)), the vertical extension of the cloud layer, its water content, and the cloud fraction are quite comparable with the LES results, except for the lowest 500 m of the cloud layer, where the cloud fraction is too large, in particular during the first 36 hours of simulation. Precipitation first occurs at 8 hours, with a precipitation rate gradually increasing up to 60 hours when it reaches approximately 0.05 mm h^{-1}, but with large fluctuations around this mean value. Note, though, that precipitation occurs at too high altitudes, in particular during the second transition phase.

However, the mean tendencies of potential temperature and water vapor mixing ratio are quite underestimated in both *1D no EDKF* and *CRM no EDKF*. This is confirmed by comparing the vertical turbulent fluxes of θ_l and r_t to those of the clouds in the LES (Figs. 13(c) and (d)). The parameterized turbulent transport remains relatively small and confined to the lowest part of the cloud layer, or even to the cloud base in *CRM no EDKF*. During the second transition phase (60 h - 90 h), in *1D no EDKF*, it compares well to the contribution of cumulus in the LES, but without any other contribution, the total turbulent transport is too weak compared to what is expected from the

LES. In *CRM no EDKF*, the very low magnitude of parameterized fluxes is partially compensated for by resolved fluxes, but the total still remains below the contribution of both cumulus and congestus in the LES.

We also know from section 5.b.1 that during the second transition phase, expected resolved fluxes at 2.5 km horizontal grid-spacing are very low. Hence, one would expect the fluxes to mainly originate from the parameterization, instead of being resolved as it is the case in *CRM no EDKF*.

4) Discussion

We have seen that the EDKF scheme may be able to simulate the turbulent fluxes and clouds associated with both cumulus and congestus clouds, but that it has difficulties representing the associated precipitation and its impact on deep convection triggering. In fact, deep convection schemes are designed to represent precipitating convection, but the KAFR scheme used here appears not to be suited to trigger before the congestus phase in this framework. As suggested by Kuang and Bretherton (2006), a unified parameterization for shallow and deep convection may be best suited to represent this gradual transition. Recent studies on continental transition cases like Suselj et al. (2019); Tang et al. (2021) show promising results with unified schemes in single-column model simulations. The trimodal parameterization evaluated in Freitas et al. (2020) including an explicit representation of the congestus regime seems also to improve the representation of the transition over land in single-column simulations.

Our analysis in section 5.b.1 revealed that simulations with kilometer-scale resolution cannot resolve the vertical turbulent fluxes associated with congestus. This further supports the need of a parameterization of both shallow cumulus and congestus clouds to properly represent the transition in cloud-resolving models. LES data have been commonly used to develop turbulence and shallow convection parameterizations (e.g. Bogenschutz and Krueger (2013); Strauss et al. (2019)), as well as to study the partition between resolved and sub-grid turbulent transport and how parameterization schemes behave across scales (Shin and Dudhia 2016; Brast et al. 2018). However we are not aware that these aspects have already been investigated up to the congestus phase.

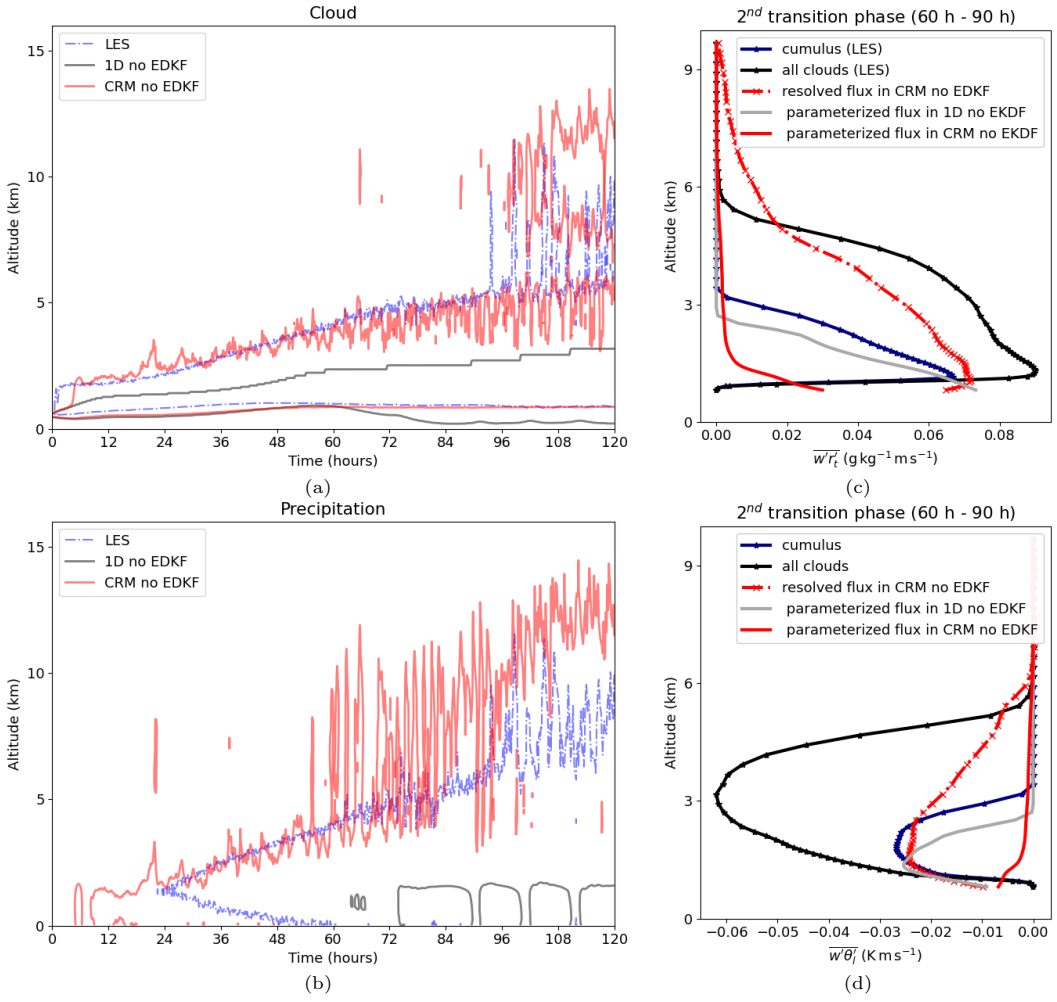

530 FIG. 13. Time evolution of the mean vertical profile of (a) cloud contour and (b) precipitation contour, in the
531 LES (blue) and *no EDKF* simulations. Cloud and precipitation contours correspond to the 10^{-6} kg kg^{-1} level of
532 respectively liquid plus ice mixing ratio and rain plus snow plus graupel mixing ratio.
533 Time average of vertical turbulent fluxes over the second transition phase of (c) total water mixing ratio and (d)
534 liquid potential temperature, diagnosed from cloud contribution in the LES, and parameterized and resolved in
535 *no EDKF* simulations.

557 The difference in response to adjustments between 1D and CRM simulations suggests that the
558 interactions between sub-grid and resolved processes play a key role, that need to be further
559 investigated. Indeed, fostering precipitation of shallow clouds inhibits convection in 1D, but
560 it enhances meso-scale organization and the formation of resolved clouds in the CRM. Spatial
561 heterogeneities might thus have an important effect on the time evolution of mean variables during

the transition, that is not taken into account in the single-column model. Parameterizations of congestus may then need to include information about the spatial distribution of clouds within a grid cell to permit a positive feedback of precipitation on deep convection development. As induced circulations in the CRM tend to have a larger horizontal extent than those in the LES, more extensive investigations are thus needed based on LES simulations to understand the underlying mechanisms. Barber et al. (2022) also underlines the need to study the spatial organization of the shallow convection at kilometer-scale resolution, and the interactions with the resolved circulation.

6. Summary and conclusions

In this paper, we simulate the idealized case of gradual transition from shallow to deep convection over ocean proposed by Kuang and Bretherton (2006) at three different horizontal resolutions. A large eddy simulation is used as a reference and serves to identify different cloud populations during this transition and to diagnose their respective contributions to turbulent transport. Simulations with kilometer-scale resolution, typical of cloud-resolving models, are used to assess the representation of transition when shallow convection is parameterized and deep convection is considered resolved. Single-column simulations are then used to evaluate the representation of convection when it is fully parameterized, such as in general circulation models used for climate projections.

The investigation of the respective contributions of the different cloud types - shallow cumulus, congestus, cumulonimbus - has shown that congestus clouds are the main contributors to the vertical turbulent fluxes of r_t and θ_l during the second half of the transition. Shallow cumulus dominate in number throughout the whole simulation, and their contribution to vertical transport remains significant even at the end of the transition and at the onset of the deep convection regime. These two aspects advocate for an adequate parameterization of congestus for the transition, although a separate scheme is not necessarily required, as well as the consideration of shallow cumulus as important contributors to turbulent transport even in the deep convection regime. Parameterizing congestus properly implies considering their vertical extent, their contribution to the vertical transport, as well as their associated precipitation. Some questions remain open. In the case of separate parameterizations for shallow and deep convection, which one of the two handles the congestus phase? And in the case of a unified parameterization, how does it behave at kilometer-scale when deep convection is mostly resolved, but most likely not the congestus phase? Congestus

are distinctly less deep and less wide than cumulonimbus, but they are also different from shallow cumulus in that they are deeper and produce more precipitation. Considering the congestus as an intermediate mode was implemented for example in Freitas et al. (2021), but also in stochastic convection parameterization where it is one of the states of a Markov chain (Dorrestijn et al. 2016; Peters et al. 2017).

Simulations with parameterized convection have revealed that the shallow convection parameterization used here does not produce sufficient rainfall, as compared to the LES. When modifying the microphysics to improve the rainfall, the effect highly differs in 1D and in CRM modes. On the one hand, in 1D, the increased rainfall inhibits the development of convection and this is also confirmed by a sensitivity test with slightly less rainfall in the shallow convection regime. This can be attributed to a uniform cooling due to evaporation. On the other hand, in CRM mode, the increased rainfall fosters resolved convection and hence the emergence of a deep convection regime. We hypothesize that the early occurrence of rainfall enhances horizontal heterogeneities, facilitating resolved circulation, which in turn increases heterogeneities. As the resolved circulation appears to be overestimated in the CRM simulation, further investigation is required to understand the physical mechanisms that should be parameterized to properly represent the transition.

Additionally, using the LES as a reference where most eddies are resolved, we calculate the expected resolved turbulent fluxes at various scales using a coarse-graining procedure and compare them to the total resolved fluxes in the LES. It has revealed that most turbulent transport is not resolved at kilometer-scale horizontal resolution. This further supports the need of parameterizing convection up to the congestus phase in kilometer-scale simulations.

The methodologies used here, in particular the approach of simulating the same case study across scales, should be applied to other cases to further investigate the role of congestus in the transition from shallow to deep convection, in particular over land where the processes are affected by the diurnal cycle and differences may arise. Our results tend to advocate for dedicated effort to develop parameterizations of convection valid for the cumulus and the congestus phases, both in kilometer-scale and large-scale models. We encourage model developers to use this case study and the methods presented here for the evaluation of the representation of the transition from shallow to deep convection, in particular the congestus phase.

Acknowledgments. We acknowledge Najda Villefranque's support in using the *htrdr* tool and Sébastien Riette's help in understanding the parameterization of microphysical processes of the shallow convection. We also acknowledge support from the DEPHY research group, funded by CNRS/INSU and Météo-France. We thank the three anonymous reviewers whose valuable comments helped us to improve the quality of the manuscript.

Data availability statement. All simulations were performed with the Meso-NH model available on http://mesonh.aero.obs-mip.fr/mesonh55. They can be consulted on request to the authors of the present paper. The code and documentation of the Monte-Carlo radiative transfer simulator *htrdr* used to obtain virtual images are available on https://www.meso-star.com/projects/htrdr/htrdr.html. Routines for the object identification are available on the Github website https://gitlab.com/tropics/objects/.

References

Barber, K. A., C. D. Burleyson, Z. Feng, and S. M. Hagos, 2022: The influence of shallow cloud populations on transitions to deep convection in the amazon. *Journal of the Atmospheric Sciences*, **79 (3)**, 723–743.

Bechtold, P., E. Bazile, F. Guichard, P. Mascart, and E. Richard, 2001: A mass-flux convection scheme for regional and global models. *Quarterly Journal of the Royal Meteorological Society*, **127 (573)**, 869–886.

Bechtold, P., J. Chaboureau, A. Beljaars, and B. N., 2014: Representing equilibrium and nonequilibrium convection in large-scale models. *jas*, **71**, 734–753.

Bechtold, P., J.-P. Chaboureau, A. Beljaars, A. Betts, M. Köhler, M. Miller, and J.-L. Redelsperger, 2004: The simulation of the diurnal cycle of convective precipitation over land in a global model. *Quarterly Journal of the Royal Meteorological Society: A journal of the atmospheric sciences, applied meteorology and physical oceanography*, **130 (604)**, 3119–3137.

Bogenschutz, P. A., and S. K. Krueger, 2013: A simplified pdf parameterization of subgrid-scale clouds and turbulence for cloud-resolving models. *Journal of Advances in Modeling Earth Systems*, **5 (2)**, 195–211.

Bougeault, P., and P. Lacarrere, 1989: Parameterization of orography-induced turbulence in a mesobeta–scale model. *Monthly weather review*, **117 (8)**, 1872–1890.

Brast, M., V. Schemann, and R. A. Neggers, 2018: Investigating the scale adaptivity of a size-filtered mass flux parameterization in the gray zone of shallow cumulus convection. *Journal of the Atmospheric Sciences*, **75 (4)**, 1195–1214.

Chaboureau, J. P., F. Guichard, J. L. Redelsperger, and J. P. Lafore, 2004: The role of stability and moisture in the diurnal cycle of convection over land. *Quarterly Journal of the Royal Meteorological Society*, **130 (604)**, 3105–3117, https://doi.org/https://doi.org/10.1256/qj.03.132, URL https://rmets.onlinelibrary.wiley.com/doi/abs/10.1256/qj.03.132.

Couvreux, F., and Coauthors, 2015: Representation of daytime moist convection over the semi-arid tropics by parametrizations used in climate and meteorological models. *Quarterly Journal of the Royal Meteorological Society*, **141 (691)**, 2220–2236.

Cuxart, J., P. Bougeault, and J.-L. Redelsperger, 2000: A turbulence scheme allowing for mesoscale and large-eddy simulations. *Quarterly Journal of the Royal Meteorological Society*, **126 (562)**, 1–30.

Deardorff, J. W., 1980: Stratocumulus-capped mixed layers derived from a three-dimensional model. *Boundary-layer meteorology*, **18**, 495–527.

Del Genio, A. D., Y. Chen, D. Kim, and M.-S. Yao, 2015: Corrigendum: The mjo transition from shallow to deep convection in cloudsat/calipso data and giss gcm simulations. *Journal of Climate*, **28 (13)**, 5471–5473.

Dorrestijn, J., D. T. Crommelin, A. P. Siebesma, H. J. Jonker, and F. Selten, 2016: Stochastic convection parameterization with markov chains in an intermediate-complexity gcm. *Journal of the Atmospheric Sciences*, **73 (3)**, 1367–1382.

D'Andrea, F., P. Gentine, A. K. Betts, and B. R. Lintner, 2014: Triggering deep convection with a probabilistic plume model. *Journal of the Atmospheric Sciences*, **71 (11)**, 3881–3901.

Fast, J. D., and Coauthors, 2019: Overview of the hi-scale field campaign: A new perspective on shallow convective clouds. *Bulletin of the American Meteorological Society*, **100 (5)**, 821–840.

Freitas, S. R., G. A. Grell, and H. Li, 2021: The grell–freitas (gf) convection parameterization: Recent developments, extensions, and applications. *Geoscientific Model Development*, **14 (9)**, 5393–5411.

Freitas, S. R., W. M. Putman, N. P. Arnold, D. K. Adams, and G. A. Grell, 2020: Cascading toward a kilometer-scale gcm: Impacts of a scale-aware convection parameterization in the goddard earth observing system gcm. *Geophysical Research Letters*, **47 (17)**, e2020GL087 682.

Guichard, F., and Coauthors, 2004: Modelling the diurnal cycle of deep precipitating convection over land with cloud-resolving models and single-column models. *Quarterly Journal of the Royal Meteorological Society: A journal of the atmospheric sciences, applied meteorology and physical oceanography*, **130 (604)**, 3139–3172.

Hohenegger, C., and B. Stevens, 2013: Preconditioning deep convection with cumulus congestus. *Journal of the Atmospheric Sciences*, **70 (2)**, 448–464.

Honnert, R., V. Masson, and F. Couvreux, 2011: A diagnostic for evaluating the representation of turbulence in atmospheric models at the kilometric scale. *Journal of the Atmospheric Sciences*, **68 (12)**, 3112–3131.

Jeevanjee, N., 2017: Vertical velocity in the gray zone. *Journal of Advances in Modeling Earth Systems*, **9 (6)**, 2304–2316.

Johnson, R. H., T. M. Rickenbach, S. A. Rutledge, P. E. Ciesielski, and W. H. Schubert, 1999: Trimodal characteristics of tropical convection. *Journal of climate*, **12 (8)**, 2397–2418.

Khairoutdinov, M., and D. Randall, 2006: High-resolution simulation of shallow-to-deep convection transition over land. *Journal of the atmospheric sciences*, **63 (12)**, 3421–3436.

Kuang, Z., and C. S. Bretherton, 2006: A mass-flux scheme view of a high-resolution simulation of a transition from shallow to deep cumulus convection. *Journal of the Atmospheric Sciences*, **63 (7)**, 1895–1909.

Kumar, V. V., C. Jakob, A. Protat, P. T. May, and L. Davies, 2013: The four cumulus cloud modes and their progression during rainfall events: Ac-band polarimetric radar perspective. *Journal of Geophysical Research: Atmospheres*, **118 (15)**, 8375–8389.

Kurowski, M. J., K. Suselj, W. W. Grabowski, and J. Teixeira, 2018: Shallow-to-deep transition of continental moist convection: Cold pools, surface fluxes, and mesoscale organization. *Journal of the Atmospheric Sciences*, **75 (12)**, 4071–4090.

Kwon, Y. C., and S.-Y. Hong, 2017: A mass-flux cumulus parameterization scheme across gray-zone resolutions. *Monthly Weather Review*, **145 (2)**, 583–598.

Lac, C., and Coauthors, 2018: Overview of the meso-nh model version 5.4 and its applications. *Geoscientific Model Development*, **11 (5)**, 1929–1969.

Lafore, J. P., and Coauthors, 1998: The meso-nh atmospheric simulation system. part i: Adiabatic formulation and control simulations. *Annales geophysicae*, Springer Verlag Göttingen, Germany, Vol. 16, 90–109.

Mechem, D. B., and S. E. Giangrande, 2018: The challenge of identifying controls on cloud properties and precipitation onset for cumulus congestus sampled during mc3e. *Journal of Geophysical Research: Atmospheres*, **123 (6)**, 3126–3144.

Panosetti, D., L. Schlemmer, and C. Schär, 2020: Convergence behavior of idealized convection-resolving simulations of summertime deep moist convection over land. *Climate Dynamics*, **55 (1-2)**, 215–234.

Park, S., 2014a: A unified convection scheme (unicon). part i: Formulation. *Journal of the Atmospheric Sciences*, **71 (11)**, 3902–3930.

Park, S., 2014b: A unified convection scheme (unicon). part ii: Simulation. *Journal of the Atmospheric Sciences*, **71 (11)**, 3931–3973.

Park, S., J. Shin, S. Kim, E. Oh, and Y. Kim, 2019: Global climate simulated by the seoul national university atmosphere model version 0 with a unified convection scheme (sam0-unicon). *Journal of Climate*, **32 (10)**, 2917–2949.

Pergaud, J., V. Masson, S. Malardel, and F. Couvreux, 2009: A parameterization of dry thermals and shallow cumuli for mesoscale numerical weather prediction. *Boundary-layer meteorology*, **132**, 83–106.

Peters, K., T. Crueger, C. Jakob, and B. Möbis, 2017: Improved mjo-simulation in echam 6.3 by coupling a s tochastic m ulticloud m odel to the convection scheme. *Journal of Advances in Modeling Earth Systems*, **9 (1)**, 193–219.

Pinty, J.-P., and P. Jabouille, 1998: A mixed-phase cloud parameterization for use in mesoscale non-hydrostatic model: simulations of a squall line and of orographic precipitations. *Conf. on cloud physics*, Amer. Meteor. Soc. Everett, WA, 217–220.

Redelsperger, J.-L., and G. Sommeria, 1981: Méthode de représentation de la turbulence d'échelle inférieure à la maille pour un modèle tri-dimensionnel de convection nuageuse. *Boundary-Layer Meteorology*, **21**, 509–530.

Rio, C., and F. Hourdin, 2008: A thermal plume model for the convective boundary layer: representation of cumulus clouds. *jas*, **65**, 407–425.

Rio, C., F. Hourdin, J.-Y. Grandpeix, and J.-P. Lafore, 2009: Shifting the diurnal cycle of parameterized deep convection over land. *Geophysical Research Letters*, **36 (7)**.

Shin, H. H., and J. Dudhia, 2016: Evaluation of pbl parameterizations in wrf at subkilometer grid spacings: Turbulence statistics in the dry convective boundary layer. *Monthly Weather Review*, **144 (3)**, 1161–1177.

Siebesma, A. P., and Coauthors, 2003: A large eddy simulation intercomparison study of shallow cumulus convection. *Journal of the Atmospheric Sciences*, **60 (10)**, 1201–1219.

Smalley, M., K. Suselj, M. Lebsock, and M. Witte, 2022: Coupling warm rain with an eddy diffusivity/mass flux parameterization: 2. sensitivities and comparison to observations. *Journal of Advances in Modeling Earth Systems*, **14 (8)**, e2021MS002 729.

Stirling, A., and R. Stratton, 2012: Entrainment processes in the diurnal cycle of deep convection over land. *Quarterly Journal of the Royal Meteorological Society*, **138 (666)**, 1135–1149.

Strauss, C., D. Ricard, C. Lac, and A. Verrelle, 2019: Evaluation of turbulence parametrizations in convective clouds and their environment based on a large-eddy simulation. *Quarterly Journal of the Royal Meteorological Society*, **145 (724)**, 3195–3217.

Suselj, K., M. J. Kurowski, and J. Teixeira, 2019: A unified eddy-diffusivity/mass-flux approach for modeling atmospheric convection. *Journal of the Atmospheric Sciences*, **76 (8)**, 2505–2537.

Suselj, K., M. Smalley, M. D. Lebsock, M. J. Kurowski, M. K. Witte, and J. Teixeira, 2022: Coupling warm rain with an eddy diffusivity/mass flux parameterization: 1. model description and validation. *Journal of Advances in Modeling Earth Systems*, **14 (8)**, e2021MS002 736.

Tang, S., P. Gleckler, S. Xie, J. Lee, M.-S. Ahn, C. Covey, and C. Zhang, 2021: Evaluating the diurnal and semidiurnal cycle of precipitation in cmip6 models using satellite-and ground-based observations. *Journal of Climate*, **34 (8)**, 3189–3210.

Tian, Y., Y. Zhang, S. A. Klein, and C. Schumacher, 2021: Interpreting the diurnal cycle of clouds and precipitation in the arm goamazon observations: Shallow to deep convection transition. *Journal of Geophysical Research: Atmospheres*, **126 (5)**, e2020JD033 766.

Villefranque, N., R. Fournier, F. Couvreux, S. Blanco, C. Cornet, V. Eymet, V. Forest, and J.-M. Tregan, 2019: A path-tracing monte carlo library for 3-d radiative transfer in highly resolved cloudy atmospheres. *Journal of Advances in Modeling Earth Systems*, **11 (8)**, 2449–2473.

Waite, M. L., and B. Khouider, 2010: The deepening of tropical convection by congestus preconditioning. *Journal of the Atmospheric Sciences*, **67 (8)**, 2601 – 2615, https://doi.org/10.1175/2010JAS3357.1, URL https://journals.ametsoc.org/view/journals/atsc/67/8/2010jas3357.1.xml.

Xu, W., and S. A. Rutledge, 2016: Time scales of shallow-to-deep convective transition associated with the onset of madden-julian oscillations. *Geophysical Research Letters*, **43 (6)**, 2880–2888.

Zhuang, Y., R. Fu, J. A. Marengo, and H. Wang, 2017: Seasonal variation of shallow-to-deep convection transition and its link to the environmental conditions over the central amazon. *Journal of Geophysical Research: Atmospheres*, **122 (5)**, 2649–2666.